International Journal of Biology and Life Sciences
ISSN: 2957-9511 | Vol. 5, No. 2, 2024

Uncovering Molecular Mechanisms of Mechanical Force Stimulation on Bone Tissue: A Bioinformatics Approach

Yiting Li [1], Zunian He [1], Jiaming Li [1], Hang Li [1], Chengliang Yang [2, *]

[1] Youjiang Medical University for Nationalities, Baise Guangxi, China
[2] Department of Orthopedic Surgery, The Affiliated Hospital of Youjiang Medical University for Nationalities, Baise, Guangxi, China
*** Corresponding author:** Chengliang Yang (Email: stbyyl@126.com)

Abstract: This study employed multiple bioinformatics approaches to uncover the potential molecular mechanisms underlying the effects of mechanical force stimulation on bone tissue. RNA sequencing data from 132 cortical bone samples were initially retrieved from the SRA database and subjected to quality control, sequence alignment, and expression matrix generation as preprocessing steps. Subsequently, WGCNA was applied for gene co-expression network analysis, followed by the selection of approximately 3,500 genes for further investigation and the exclusion of outliers. Clustering and correlation analyses revealed sets of genes highly associated with mechanical force stimulation. To gain insight into the functional characteristics of these genes, PPI network construction and GO and KEGG enrichment analyses were performed. Results indicated distinct functional properties of different modules under various conditions. For instance, genes within the MEsalmon module were mainly associated with actin cytoskeleton and calmodulin in response to mechanical force stimulation; whereas genes within the MEbrown module, when considering growth plates and other skeletal regions, primarily involved ribosomal proteins and energy metabolism. With prolonged treatment time, genes within the MEblack module exhibited increased energy metabolic activity. These findings suggest that mechanical force stimulation can alter the expression levels of specific genes in bone tissue, thereby affecting their biological functions. This study provides a new perspective on how mechanical force stimulation regulates bone tissue and may have positive implications for therapeutic strategies in fracture healing and bone diseases.

Keywords: Mechanical Force Stimulation; Gene Co-expression Network Analysis; Bone Tissue.

1. Introduction

Mechanical force stimulation can exert effects on various tissues of organisms. Mechanical loading is regarded as a pivotal factor in bone development and maintenance, accomplished by activating osteoblasts and reducing osteoclast activity, ultimately leading to increased bone mass via stimulation of bone formation and inhibition of bone resorption [1]. Biomechanical stimulation is crucial for the induction of chondrogenesis, particularly in the treatment of osteoarthritis [2]. Upon exposure to mechanical stimuli, muscles instantaneously elicit a response involving alterations in intracellular calcium ion concentration, activation of myosin light chain kinase, and transcriptional regulation of genes associated with muscle contraction, ultimately leading to adaptation of the muscle to various exercise demands [3]. The nervous system is also influenced by mechanical stimulation [4].

Distraction osteogenesis (DO), a common approach for treating nonunion and bone defects, has been widely applied in limb reconstruction in orthopedics and craniofacial reconstruction in maxillofacial surgery [5-6]. The principle underlying this technology is the effect of mechanical force stimulation on bone tissue.

The underlying mechanisms by which mechanical stimuli regulate bone tissue remain unclear, warranting further investigation. In this study, we employed the methods of WGCNA, PPI construction, GO enrichment analysis, and KEGG enrichment analysis to investigate the underlying mechanism by which mechanical force stimulation affects bone tissue.

2. Materials and Methods

2.1. Acquisition of SRA Sequencing Sequences

Original sequence data for SRP390721 were obtained from the SRA database (https://www.ncbi.nlm.nih.gov/sra/). The dataset SRP390721 encompasses ribonucleic acid sequencing (RNA-seq) data from 132 cortical bone [7]. Cortical bone from the loaded limb and contralateral control limb of tibiae in 10-week-old female C57 mice following mechanical loading (1 hour, 3 hours, 24 hours, 5 days, 7 days) were examined. The cortical bone was then divided into three regions: the diaphyseal cortex, proximal metaphyseal shell, and mid-diaphyseal cortex.

2.2. Sequence Alignment and Expression Matrix Generation

The reference genome for sequence alignment was the Mus_musculus. GRCm39.110 dataset, which was released by the Ensembl database in July 2023 [8]. The fastQ files of the SRP390721 dataset were subjected to quality control using the fastp software [9]. Index files were generated using the maximum length value of 75 for annotating variable splicing sequences with the STAR software, and sequence alignment was performed using the STAR software to produce alignment result files [10]. Quantification of the number of individual genes was performed using the RSEM software on the resulting sequence alignment files [11]. The integrated data were formatted into a gene expression matrix for subsequent analysis.

2.3. Weighted Gene Co-expression Network Analysis

The expression matrix derived from the aforementioned processing was imported into the R environment for analysis and visualization [12]. Variance-stabilizing transformation (VST) normalization of the aforementioned expression matrix was performed using the DESeq2 software [13].

Approximately 3,500 genes with values within the top 10% of standard deviation were selected for WGCNA analysis [14]. Using 81 as the cutoff value, outliers were excluded. With an R-square value of 0.9, the soft threshold was selected. Employing the soft thresholding approach, transpose the expression matrix into an adjacency matrix, which is then transformed into a topological overlap matrix (TOM). The dissimilarity of the TOM (dissTOM) is subsequently calculated. Clustering is performed utilizing the dissTOM for cluster formation and a dendrogram is plotted to illustrate these clusters. Setting a minimum gene threshold of 30 genes per module, a Dynamic Tree Cut is generated and individual module colors are defined. Eigengenes are computed, with a MEDissThres value set at 0.25, allowing for the merging of similar modules within the clustering tree.

We calculated the correlation between modules and trait information, and identified modules with high correlation coefficients ($P < 0.05$) across different trait information. The gene sets of these identified modules were used as data sources for subsequent analyses.

2.4. Constructing Protein-Protein Interaction Networks (PPI) in Module Genes to Identify Hub Genes

The gene set with high correlation to the Trait information was input into the STRING database for PPI data inquiry, and unconnected nodes were removed [15]. The obtained PPI data was then imported into the Cytoscape software, where the NCC score was calculated using the cytoHubba plugin of the Cytoscape software, and the top 10 genes were selected for display [16-17].

2.5. Conduct GO and KEGG Enrichment Analysis for Genes Within the Modules

Enrichment analysis was performed using the clusterProfiler software with a significance level set at $P < 0.05$ [18]. Conducting Gene Ontology (GO) enrichment analysis with the gene set obtained from the module highly correlated with Trait information, present the enriched Biological Process (BP), Cell Component (CC), and Molecular Function (MF) terms. Conduct Kyoto Encyclopedia of Genes and Genomes (KEGG) enrichment analysis on the module gene sets obtained above with high correlation to Trait information, presenting the enriched pathway names.

3. Results

3.1. WGCNA

Using 81 as the cutoff value, outliers were excluded (Figure 1 A-B). A soft thresholding power of 16 was selected, yielding an R-squared value of 0.91 when assessing the scale-free topology, indicating that the scale-free network met the requirements (Figure 1 C-D). Conducting agglomeration of similar modules, we ultimately obtained the Gene dendrogram and module colors (Figure 1 E-F). Among these, the MEgrey module comprises genes that could not be classified into any specific module.

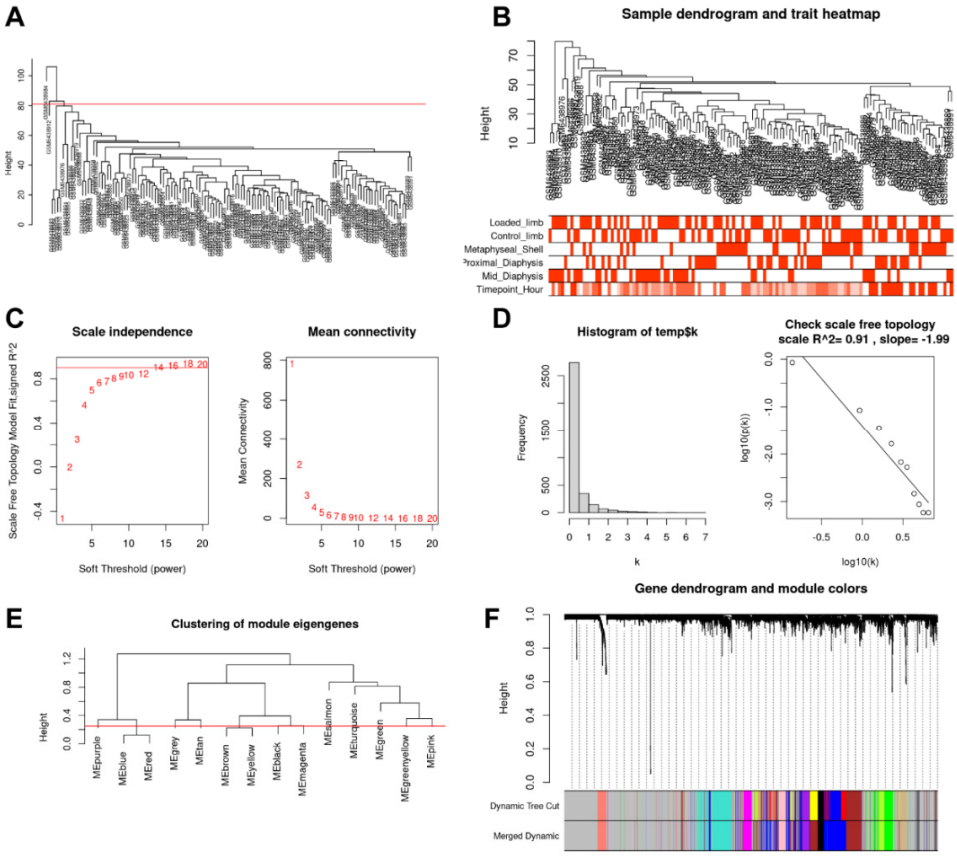

Figure 1. Distinguishing modules in WGCNA, (A) outliers were excluded, (B) distributions of trait information across different samples, (C-D) selection of the soft threshold value, (E) the basis for clustering similar modules, (F) gene dendrogram and module colors.

Calculate the correlation coefficient between genes in the module and trait information to obtain a heatmap of the correlation between the module and trait information (Figure 2 A). When limb loading was used as an influencing factor, the absolute value of the correlation coefficient for the MEsalmon module was the largest at 0.22 and demonstrated significant differences (Figure 2 B). The epiphyseal region serves as the center for osteogenesis, with its growth and development affecting bone quality changes throughout the tibia. When the epiphyseal corticular status was used as an influencing factor, the MEbrown module exhibited a negative correlation with significant differences (Figure 2 C). MEblack displayed a positive correlation and significant difference in the continuous variable Timepoint_Hour, suggesting upregulation of this module over time (Figure 2 D).

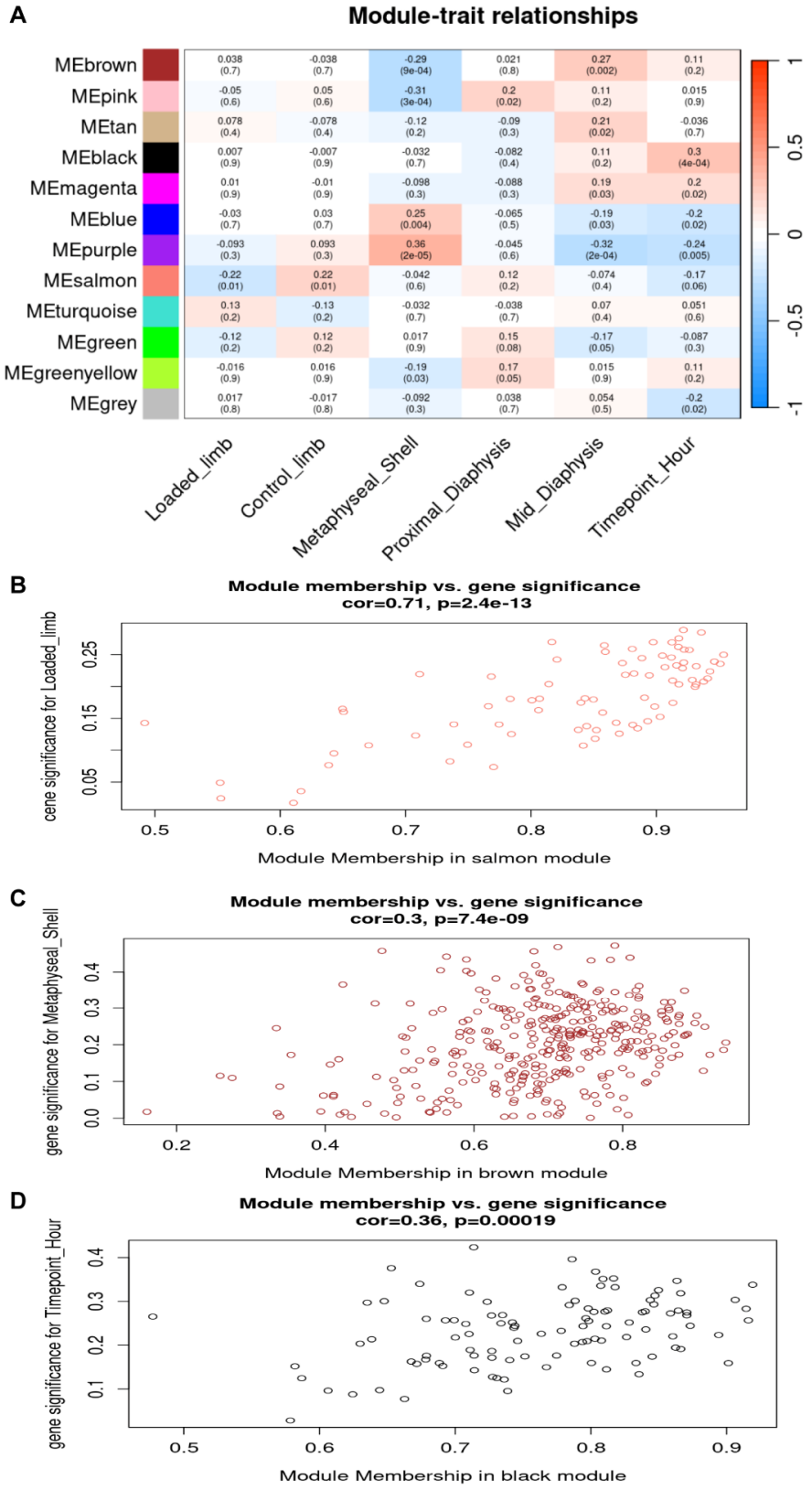

Figure 2. Module-trait relationships, (A) all module-trait relationships, (B) MEsalmon module membership vs. Loaded_limb, (C) MEbrown module membership vs. Metaphyseal_Shell, (D) MEblack module membership vs. Timepoint_Hour

3.2. Constructing PPI in Module Genes to Identify Hub Genes

To identify key genes associated with Loaded, the top 77 genes from the MEsalmon module were imported into the STRING database for PPI network analysis. Unconnected nodes were removed, resulting in a network consisting of 66 genes. Within this PPI interaction network, the top 10 genes with the highest NCC scores were Casq1, Mybpc2, Atp2a1, Actn3, Tnnt3, Tnni2, Ttn, Tnnc2, Acta1, and Myl1 (Figure 3 A).

Using the MEbrown module consisting of 355 genes, we queried the PPI network in the STRING database and removed unconnected nodes, resulting in 296 genes. Among the PPI interaction network, the top 10 genes with the highest NCC scores were Rpl31, Rpl34, Rpl30, Rpl36al, Rpl4, Rpl32, Rps18, Rps6, Rps21, and Rps23, primarily related to ribosomal proteins. Ribosomes are mainly responsible for translating genetic information from nucleic acids into proteins, suggesting that protein synthesis is robust in the cortices of both growth plates and other cortices of bones (Figure 3 B).

To construct the PPI network for the 98 genes in the MEblack module, these genes were imported into the STRING database, and unconnected nodes were removed, resulting in 57 genes. Among the top 10 genes with the highest NCC scores in the PPI interaction network were Cox6a1, mt-Nd4, mt-Nd2, Cox5b, Ndufv3, Ndufc2, mt-Cytb, Blvrb, Ubb, and mt-Atp6. Several mitochondrial-related genes were identified among these, as mitochondria play a crucial role in providing energy to cells. This suggests that as mechanical stimulation time increases, cellular metabolism becomes more robust (Figure 3 C).

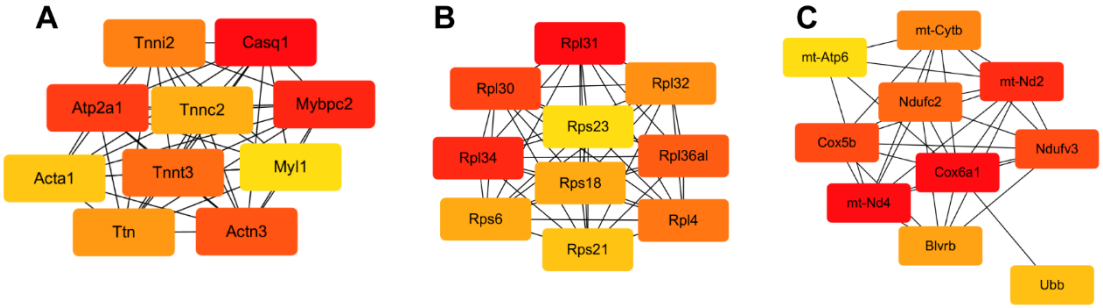

Figure 3. In different modules, the top 10 genes with the highest NCC scores are displayed, with darker colors representing higher NCC scores, (A) MEsalmon module, (B) MEbrown module, (C) MEblack module

3.3. GO Enrichment Analysis and KEGG Enrichment Analysis

In the MEsalmon module, the results of GO enrichment analysis were primarily concentrated on items related to troponin and the cytoskeleton, while the results of KEGG enrichment analysis were mainly focused on items associated with troponin movement (Figure 4 A-B).

In the MEbrown module, the results of GO enrichment analysis were predominantly focused on entries related to ribosomal proteins and energy metabolism, while the normal physiological pathways in KEGG enrichment analysis were primarily concentrated on entries associated with oxidative phosphorylation and Tight junction (Figure 4 C-D).

Within the MEblack module, the results of Gene Ontology enrichment analysis were primarily concentrated on entries related to aerobic respiration and mitochondrial ATP synthesis transmission, while the normal physiological pathways identified through KEGG enrichment analysis were oxidative phosphorylation and Retrograde endocannabinoid signaling (Figure 4 E-F).

4. Discussion

In this study, the results of PPI, GO enrichment, and KEGG enrichment analyses from the MEsalmon module revealed that mechanical stimulation influences alterations in troponin and cytoskeleton components in cortical bone, reflecting adaptive responses within the bone tissue. In the context of tension-induced osteogenesis, the application of mechanical force stimuli exerts an influence on bone tissue, thereby promoting bone tissue regeneration and angiogenesis [19, 20]. The process of tension-induced osteogenesis is precisely due to the activation of tropomyosin and cytoskeleton-related pathways, which subsequently provoke alterations in a series of subsequent physiological activities.

Analysis of the MEbrown module revealed distinct metabolic activities between the Metaphyseal Shell and other cortices, with the Metaphyseal Shell exhibiting enhanced ribosomal protein synthesis and energy metabolism compared to other cortices, indicative of greater osteogenic activity in the Metaphyseal Shell. The fundamental distinction between growth plates and other skeletal regions lies in the fact that growth plates, located at the ends of developing long bones, are responsible for linear bone growth. Composed of cells referred to as chondrocytes, which secrete extracellular matrix and are arranged functionally, growth plates lack direct blood supply except for the presence of cartilage vasculature in larger mammals; instead, solutes are transported to the cartilage via vessels surrounding it. Throughout different stages of growth, chondrocytes undergo coordinated and sequential differentiation, eventually undergoing hypertrophy and cell death. Subsequently, the cartilage template is replaced by osteoclasts and osteoblasts originating from invading vessels, giving rise to true bone.

In the analysis of the MEblack module, it was demonstrated that as the duration of mechanical force stimulation increases, the energy metabolism of cortical bone becomes more robust. Mechanical force stimulation can enhance the metabolic activity of bone tissue, thereby promoting both osteogenic and osteoclastic activities, ultimately achieving bone tissue remodeling. Thus, maintaining appropriate mechanical force stimulation over an extended period is beneficial to bone tissue. This is also the reason why exercise is beneficial to bone tissue [21].

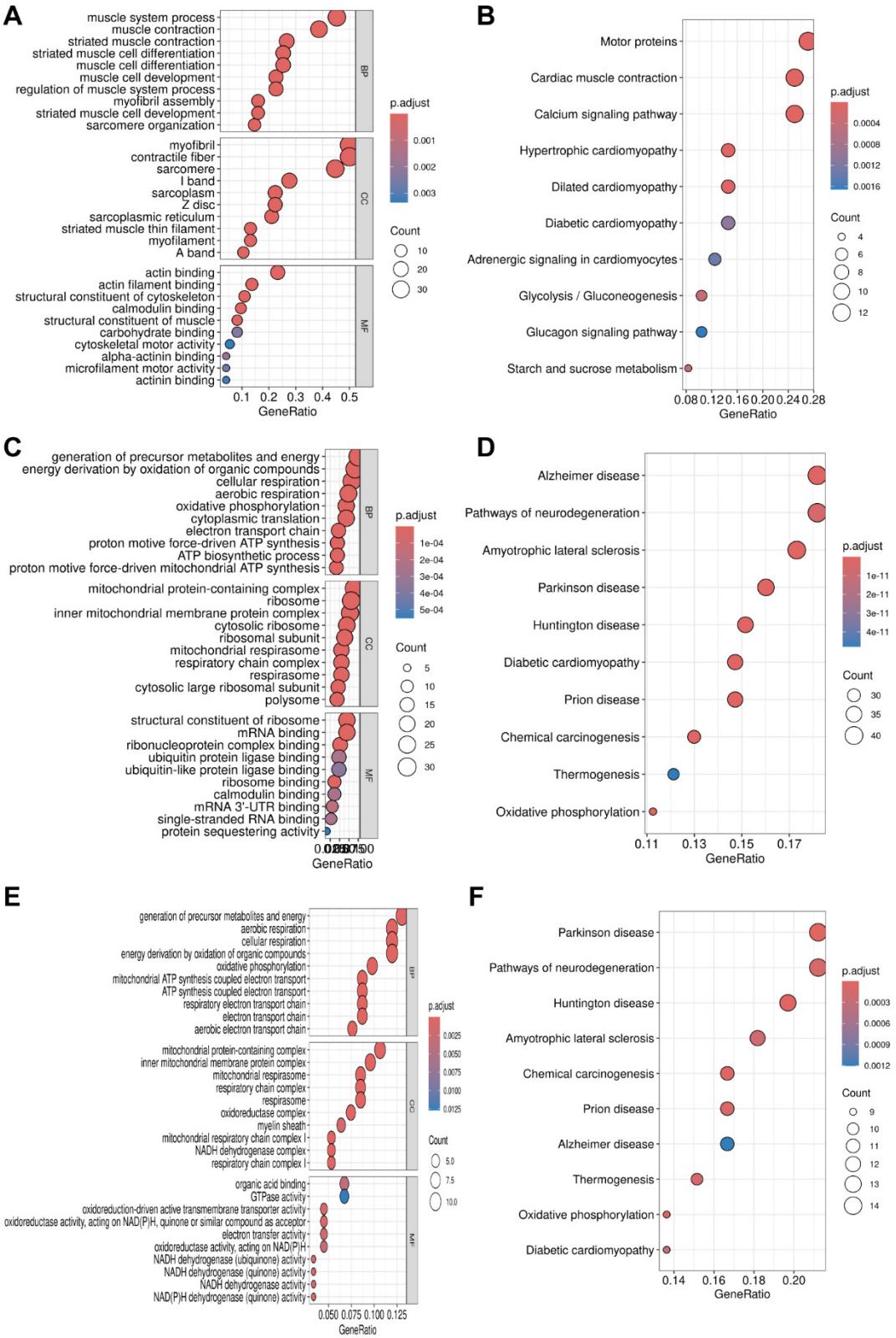

Figure 4. The enrichment analysis results of GO and KEGG in different modules, (A-B) MEsalmon module, (C-D) MEbrown module, (E-F) MEblack module

In the present study, in vitro or in vivo experiments were not conducted to validate the findings, which warrants further improvement in future research.

In the research of exploring the mechanism of mechanical force stimulation on bone tissue, more emphasis should be placed on the changes in cytoskeleton and cell junctions. Meanwhile, an enhancement in metabolism with prolonged duration of mechanical force stimulation constitutes a novel research perspective.

References

[1] Cai F, Yusufu A, Liu K, et al. High-fat diet causes undesirable bone regeneration by altering the bone marrow environment in rats. Front Endocrinol (Lausanne). 2023;14:1088508. doi:10.3389/ fendo.2023.1088508.

[2] Niemeyer F, Claes L, Ignatius A, Meyers N, Simon U. Simulating lateral distraction osteogenesis. PLoS One. 2018; 13(3): e0194500. doi:10.1371/journal.pone.0194500.

[3] Shilnikov V, Denisov A, Masueva K. The optimization of the length of the lower limbs after hip arthroplasty. Int Orthop. 2019; 43(11):2485-2490. doi:10.1007/s00264-019-04395-x.

[4] Brazill JM, Beeve AT, Craft CS, Ivanusic JJ, Scheller EL. Nerves in Bone: Evolving Concepts in Pain and Anabolism. J Bone Miner Res. 2019;34(8):1393-1406. doi:10.1002/ jbmr. 3822.

[5] Huang C, Holfeld J, Schaden W, Orgill D, Ogawa R. Mechanotherapy: revisiting physical therapy and recruiting mechanobiology for a new era in medicine. Trends Mol Med. 2013;19(9):555-564. doi:10.1016/j.molmed.2013.05.005.

[6] Durham JN, King JW, Robinson QC, Trojan TM. Long-term skeletodental stability of mandibular symphyseal distraction osteogenesis: Tooth-borne vs hybrid distraction appliances. Angle Orthod. 2017;87(2):246-253. doi:10.2319/022916-175. 1.

[7] Chlebek C, Moore JA, Ross FP, van der Meulen MCH. Molecular Identification of Spatially Distinct Anabolic Responses to Mechanical Loading in Murine Cortical Bone. J Bone Miner Res. 2022;37(11):2277-2287. doi:10.1002/ jbmr. 4686.

[8] Martin FJ, Amode MR, Aneja A, et al. Ensembl 2023. Nucleic Acids Res. 2023;51(D1):D933-D941. doi:10.1093/ nar/ gkac 958.

[9] Chen S. Ultrafast one-pass FASTQ data preprocessing, quality control, and deduplication using fastp. iMeta. 2023;2(2):e107. doi: 10.1002/imt2.107.

[10] Dobin A, Davis CA, Schlesinger F, et al. STAR: ultrafast universal RNA-seq aligner. Bioinformatics. 2013;29(1):15-21. doi:10.1093/bioinformatics/bts635.

[11] Li B, Dewey CN. RSEM: accurate transcript quantification from RNA-Seq data with or without a reference genome. BMC Bioinformatics. 2011; 12:323. doi:10.1186/1471-2105-12-323.

[12] R Core Team. R: A Language and Environment for Statistical Computing. Published online 2023. https://www.R-project.org/.

[13] Love MI, Huber W, Anders S. Moderated estimation of fold change and dispersion for RNA-seq data with DESeq2. Genome Biol. 2014;15(12):550. doi:10.1186/s13059-014-0550-8.

[14] Langfelder P, Horvath S. Fast R Functions for Robust Correlations and Hierarchical Clustering. J Stat Softw. 2012; 46 (11):i11.

[15] Szklarczyk D, Kirsch R, Koutrouli M, et al. The STRING database in 2023: protein-protein association networks and functional enrichment analyses for any sequenced genome of interest. Nucleic Acids Res. 2023;51(D1):D638-D646. doi:10. 1093/nar/gkac1000.

[16] Chin CH, Chen SH, Wu HH, Ho CW, Ko MT, Lin CY. cytoHubba: identifying hub objects and sub-networks from complex interactome. BMC Syst Biol. 2014;8 Suppl 4(Suppl 4): S11. doi:10.1186/1752-0509-8-S4-S11.

[17] Shannon P, Markiel A, Ozier O, et al. Cytoscape: a software environment for integrated models of biomolecular interaction networks. Genome Res. 2003;13(11):2498-2504. doi:10.1101/ gr.1239303.

[18] Wu T, Hu E, Xu S, et al. clusterProfiler 4.0: A universal enrichment tool for interpreting omics data. Innovation (Camb). 2021;2(3):100141. doi: 10.1016/j.xinn.2021.100141.

[19] Du GQ, Gong ZH, Liang B, et al. Concentration Changes of Peripheral Blood Mesenchymal Stem Cells of Sprague Dawley Rats during Distraction Osteogenesis. Orthop Surg. 2021;13(2): 623-631. doi:10.1111/os.12823.

[20] Ou S, Xu C, Yang Y, et al. Transverse Tibial Bone Transport Enhances Distraction Osteogenesis and Vascularization in the Treatment of Diabetic Foot. Orthop Surg. 2022;14(9):2170-2179. doi:10.1111/os.13416.

[21] Salhotra A, Shah HN, Levi B, Longaker MT. Mechanisms of bone development and repair. Nat Rev Mol Cell Biol. 2020; 21 (11): 696-711. doi:10.1038/s41580-020-00279-w.